



CHORUS

This is the accepted manuscript made available via CHORUS. The article has been published as:

Atomic migration and bonding characteristics during a glass transition investigated using as-cast Zr-Cu-Al

C. Fan, Y. Ren, C. T. Liu, P. K. Liaw, H. G. Yan, and T. Egami

Phys. Rev. B **83**, 195207 — Published 11 May 2011

DOI: [10.1103/PhysRevB.83.195207](https://doi.org/10.1103/PhysRevB.83.195207)

Atomic migration and bonding characteristics during glass transition

- investigated by a as-cast Zr-Cu-Al

C. Fan^{1*}, Y. Ren², C. T. Liu³, P. K. Liaw⁴, H. G. Yan¹, and T. Egami⁴

¹ *College of Materials Science and Engineering, Hunan University, Changsha 410082, P.R. China*

² *X-ray Science Division, Argonne National Laboratory, Argonne, Illinois 60439, USA*

³ *Mechanical Engineering Department, Hong Kong Polytechnic University, Hung Hom, Kowloon, Hong Kong*

⁴ *Department of Materials Science and Engineering, The University of Tennessee, Knoxville, TN 37996, USA*

* fan@hnu.edu.cn

Abstract

The glass transition involves a minor change in the internal energy, and yet the physical and mechanical properties of a glass change dramatically. Atomic bonding behavior is critical to understanding these interesting changes. In order to determine the evolution of the atomic structure through the glass transition, we employed *in-situ* synchrotron x-ray scattering measurements as a function of temperature on a model material – Zr-Cu-Al metallic glass. Based upon the study of pair distribution function and the characterization of the free volume in terms of atomic bonding lengths, we found that the relative change of the quantity, $\Delta N/N$ (N represents the number of atom pairs) with significantly longer interatomic distances for the nearest atomic pairs, increases abruptly above the glass transition temperature (T_g). These phenomena are interpreted in terms of the tight-bond cluster model developed recently.

I. INTRODUCTION

Liquids existing at temperatures far below their melting point are commonly referred as "supercooled" liquids. Supercooled liquids show a rapid increase in viscosity with cooling, and further cooling to below the glass transition temperature (T_g) produces a glassy phase. The glass transition results in dramatic changes in their physical and mechanical properties, even though the change in the internal energy is minor^[1-6]. The glass transition behavior has been studied mostly on dynamics and thermodynamics of molecular glass materials ^[1, 3, 7, 8], and few investigations directly examined the changes in the atomic structure mainly because of the complexity in the atomic structure of molecular glasses. Metallic glasses are simpler in the sense that the structural unit is an atom. They are of interest to scientists due to their unique physical, chemical, and mechanical properties. However, metallic glasses have been less stable than molecular glasses, and many of them crystallize around the glass transition temperature, making it difficult to study their behavior through the glass transition. But extensive efforts of recent studies have led to breakthroughs ^[4, 5, 9, 10] on improving the glass forming ability ^[4, 5, 11, 12] with the critical cooling rate decreasing from $> 10^5$ K/s for regular metallic glasses to $\sim 10^0$ K/s for certain bulk metallic glasses (BMGs). Thus, we now have a possibility to study their structural evolution through the glass transition by diffraction, which is the subject of this work. In this paper, we describe the subtle changes in the atomic pair distribution function (PDF) observed by *in-situ* synchrotron x-ray scattering measurements at temperatures from room temperature to above T_g .

II. EXPERIMENTAL

In this investigation, the atomic pair-distribution functions (PDF) analysis was used to determine the local atomic structure of a $Zr_{55}Cu_{35}Al_{10}$ (atomic percent) bulk metallic glass (BMG). The ingots were fabricated by arc-melting, using high purity elements. Samples were subsequently produced by suction-casting in a copper mold (1 mm thick plate for synchrotron measurements and 3 mm in diameter rods for neutron measurements). The T_g of this glass is 420 °C, whereas the crystallization temperature, T_x , is 492 °C, as observed by differential scanning calorimetry (DSC) at heating rate of 20 °C/min. This significant difference between T_g and T_x made it possible to observe the structural change through T_g by *in-situ* synchrotron x-ray diffraction without crystallization.

The PDF data were induced from the *in-situ* synchrotron x-ray diffraction measurements with an average specimen heating rate of about 20 °C/min, carried out at the beamline 11 D of the Advanced Photon Source (APS), Argonne National Laboratory. In addition, pulsed neutron PDF measurements were done at room temperature on the as-cast and crystallized samples, with the Neutron Powder Diffractometer (the NPDF spectrometer) of the Lujan Center of Los Alamos National Laboratory. The schematic diagram for the *in-situ* synchrotron x-ray diffraction measurements is shown in Fig. 1. Incident photons past through the heated specimen and were recorded on the image plate detector to form a 2-D (two dimensional) image pattern. The high penetration depth and fast data generation rates of these measurements allowed us to obtain structural changes

between data collections at designed temperatures over a wide temperature range of the supercooled liquid region, $\Delta T_x (= T_x - T_g)$ with continuous heating.

The diffraction data, $I(Q)$, was collected over a wide range of Q (over 30 \AA^{-1} , where $Q = (4\pi \sin \theta) / \lambda$, θ is the diffraction angle, and λ is the x-ray wavelength). Subsequently, the PDF, $G(r)$ vs. r , where r is the distance between atomic pairs, was computed using the program PDFgetX2 [13] or PDFgetN [14] for data reduced by synchrotron x-ray diffraction or neutron scattering, via the Fourier transform of $Q[S(Q) - I]$, where $S(Q)$ is the total scattering structure function:

$$G(r) = 4\pi r \rho_0 [g(r) - 1] = \frac{2}{\pi} \int [S(Q) - 1] \sin(Qr) Q dQ \quad (1)$$

III. RESULTS

To investigate the temperature dependence of the structure through the glass transition, *in-situ* synchrotron x-ray scattering measurements for the as-cast $\text{Zr}_{55}\text{Cu}_{35}\text{Al}_{10}$ BMG were carried out over a range of sample temperatures, from room temperature (RT) to $450 \text{ }^\circ\text{C}$, which is above T_g ($420 \text{ }^\circ\text{C}$) but sufficiently below T_x to avoid crystallization during the measurement. Figure 2(a) shows the structure function, $S(Q)$, at RT and $450 \text{ }^\circ\text{C}$. The two curves are almost overlapped and the difference is quite small. It indicates that the specimen has the amorphous characters during testing at $450 \text{ }^\circ\text{C}$. In comparison, the change in $S(Q)$ due to only a partial crystallization (a very early crystallization stage)

is much more extensive - not only the intensity of their peaks increased significantly, but also their peaks separated into multi-narrow peaks, as shown in Fig. 2(b).

PDF presents the atomic pair information in real space. It presents more detailed and intensive changes in short- and medium- range neighbor atoms, which is sensitive to defects, as compared with $S(Q)$. The nearest neighbor peaks of PDF provide detailed information about the short-range order, which is the primary correlation among atoms in the glass. Figure 3(a) shows the nearest neighbor peak of the PDF curves, $G(r)$, at RT and $450\text{ }^{\circ}\text{C}$. Changes in $G(r)$ are slightly more prominent than those in $S(Q)$. For instance, the first peak in $G(r)$ measured at $450\text{ }^{\circ}\text{C}$ is considerably wider than that measured at RT . The change in the PDF due to crystallization is dramatic, as shown in Fig. 3(b), which was obtained by pulsed neutron scattering measurements at RT . The crystallized sample was annealed at about $700\text{ }^{\circ}\text{C}$ for 3 hours (for obtaining stable crystallized phases), and the main crystallized phase is CuZr_2 . The width of this peak is much larger for the glass sample compared to the crystallized sample, reflecting the wider range in the bond length distribution in the glassy state. Due to the difference of the synchrotron x-ray scattering and neutron scattering, the PDF intensities are different between Figs. 3(a) and (b) for the same amorphous alloy.

A part of the changes of the *in-situ* PDF data as a function of temperature is due to atomic bonding expansion. In order to characterize this effect, we evaluated the temperature dependence of the average nearest neighbor distance, \bar{r} , from RT to $450\text{ }^{\circ}\text{C}$, using the center-of-mass method,

$$\bar{r} = \frac{\int_{r_L}^{r_H} [R(r) \cdot r] r^2 dr}{\int_{r_L}^{r_H} R(r) r^2 dr} \quad , \quad (2)$$

where, $R(r)$ is the radial distribution function (RDF), $R(r) = 4\pi r^2 \rho_0 g(r) = rG(r) + 4\pi r^2 \rho_0$, and we chose $r_L = 2.14 \text{ \AA}$ and $r_H = 3.89 \text{ \AA}$ at room temperature to cover the entire first peak. The slope, $\alpha_a = \Delta\bar{r} / \bar{r}_0$, the thermal expansion at the atomic level, is $1.2 \times 10^{-5} \text{ }^\circ\text{C}^{-1}$ from RT to $370 \text{ }^\circ\text{C}$ (below T_g), as shown in Fig. 4. The thermal expansion at the atomic level is significantly lower than the value of α , which is the measured value of linear thermal expansion coefficient at room temperature, $\alpha = 3.275 \times 10^{-5}$. Actually such a difference between the macroscopic and microscopic coefficient is fairly common even for crystals.

When temperatures are above T_g , as shown in Fig. 4, for the range from 420 to $450 \text{ }^\circ\text{C}$, the slope $\alpha_{scl} = \Delta\bar{r} / \bar{r}_0$ increases to 2.3×10^{-5} , which is twice of α_a ($\alpha_{scl} / \alpha_a \approx 2$). The increase in the slope above T_g indicates extra volume expansion as expected for a liquid above the glass transition due to configurational changes in the topology of the atomic connectivity network.

In order to evaluate the effect of peak broadening, the number of atom pairs in the tails of the first peak was calculated by the following equation

$$N = \int_{r_1}^{r_2} R(r) dr \quad (3)$$

The quantity of $R(r)dr$ gives the number of atoms in an annulus of thickness dr at a distance r from another atom. In Fig. 3(a), when $r_1 = 3.55 \text{ \AA}$ and $r_2 = 3.89 \text{ \AA}$, the quantity

N represents the number of atom pairs with the significantly longer interatomic distances compared with 3.24 Å, which is the atomic distance of the nearest Zr-Zr pair in crystalline solutions (Zr is the largest atom in Zr-Cu-Al system).

As described above, $r_2 = 3.89$ Å is to cover the entire peak of the nearest neighbor pairs in the PDF curve. Choosing $r_1 = 3.55$ Å for estimating N is based on Lindemann's Melting Criterion. The first theory explaining mechanism of melting in the bulk was proposed by Lindemann [15], who used vibration of atoms in the crystal to explain the melting transition. The average amplitude of thermal vibrations increases when the temperature of the solid increases. At a certain point, the amplitude of vibration becomes so large that the atoms start to invade the space of their nearest neighbors and disturb them and the melting process initiates. Quantitative calculations based on the model are not easy, hence Lindemann offered a simple criterion: melting might be expected when the root mean vibration amplitude $\sqrt{\langle \mu^2 \rangle}$ exceeds a certain threshold value (namely when the amplitude reaches at least 10% of the nearest neighbor distance). In the Zr-Cu-Al system, atom Zr has the largest atomic size, and the Zr-Zr atomic distance in crystalline solution is 3.24 Å. The chosen atomic pair distance of $r_1 = 3.55$ Å is ~10% larger than 3.24 Å.

Even the above cutoff are somewhat arbitrarily chosen around the 10%, it has no much effect on the results since we are interested in the relative change of this quantity, $\Delta N/N_0$, where $\Delta N = N(T) - N_0$, N_0 is the number of atom pairs in the range of r_1 and r_2 at room temperature. The normalized $\Delta N/N_0$ of the RDFs from 3.55 to 3.89 Å is shown in Fig. 5(a). The slope ($B_{scl} = 9.7 \times 10^{-2}$) of the $\Delta N/N_0$ above T_g , which is more than twice

that below T_g ($B_a = 4.0 \times 10^{-2}$), increases abruptly above T_g . The ΔN means the differences of the number of atoms between traveling in and out of the r_1 to r_2 zone as shown in Fig. 5(b). The ration of $B_{scl} / B_a = 2.4$ indicates that atoms that enter into the r_1 to r_2 zone above T_g is 2.4 times of that below T_g .

IV. DISCUSSION

As shown in Fig. 4(a), the atomic bonding expansion significantly increases above T_g . It is possible to speculate that the large value of α_{scl} compared to α_a , may reflect the partially liquid-like nature of the glass structure. According to Ref ¹⁶ and ¹⁷, it is likely that the atomic structure does not change from solid to liquid at the glass transition [^{16, 17}]. The structure of a glass is not uniform, but includes both solid-like and liquid-like local structures. The glass transition manifests itself through the percolation of the liquid-like local structures. Thus, the liquid-like structure should show the thermal expansion due to both the potential anharmonicity and configurational change, resulting in a larger than that of the solid-like structures.

In the free-volume theory [^{16, 18}] the liquid-like cells are defined by the excess amounts of free-volumes. The free-volume theory has been widely used in the metallic glass community. However, the authors of the theory warned against its use in metallic systems, because the critical size of the free volume, γ^*/v_0 , where v_0 is the atomic volume, is only about 0.1, whereas it is about 0.8 for hard-sphere systems for which the theory was designed [¹⁸]. Indeed metallic atoms are not hard-sphere-like, and is easily

deformable, making it difficult to apply the free-volume theory in its original form [19-22].

Free volume can be defined as a negative deviation in the local atomic density.

In the metallic systems, the distribution in local atomic volumes is more harmonic, close to the Gaussian distribution [23], ranging from negative to positive deviations from the average. From the theory based on the atomic level stresses [24], it was mentioned that the local structural variation results not only in the free volume-like low density regions (n-type local density fluctuations), but also in the compressed high density regions (p-type local density fluctuations) [25]. In terms of the critical local volume strain of ε_v , the glass transition can be defined by the density of the atomic sites with the local volume strain larger than the critical value. The critical local volume strain is 0.11 [17], this meaning that if the local transformation volume strain is larger than 11% or smaller than -11%, the site is topologically unstable. When using the $\varepsilon_v = 0.11$, the values of T_g , thus calculated for a large number of metallic glasses, agree well with the experimental data [17].

The energy, E , is a function of the atomic positions, r , of all the atoms in the system and temperature. A sum of internal (or bonded) terms, E_{bonded} , which describe the bonds, angles and bond rotations in a molecule or cluster, is the main factor of the E . The E_{bonded} term is thus a sum of three terms:

$$E_{bonded} = E_{bond-stretch} + E_{angle-bend} + E_{rotate-along-bond}$$

The first term $E_{bond-stretch}$ in the above equation, which is a harmonic potential energy representing the interaction between atomic pairs, is strongly related to the energy of a bond as a function of displacement from the ideal bond length. The most recent studies [19-22] from PDFs of BMGs have pointed out that free volumes are resulted from these atom pairs that have longer bond lengths than that in the solid solution but normally not long enough to fill in an atom, this making the free volume concept being more clear.

Figure 3(b) shows that some of the atomic pairs have their pair distance significantly smaller than those in the annealed crystalline materials. This feature indicates that the clusters in BMGs consist of compressively bonded atoms. Figure 3(b) also shows that some of the atomic pairs have their pair distance significantly longer than those in the annealed crystalline materials. It indicates that BMGs also contain a certain amount of free volumes. The clusters with compressed bonds and the free volume with loose bonds coexist in a BMG. Consequently, based on Lindemann's Melting Criterion, it is reasonable to consider that the atom pairs having a distance longer than 3.55 Å (= r_1 in Fig. 5) and less than 3.89 Å (= r_2 , the end of the distance for nearest pairs) form free volumes in this alloy since the atomic pair distance >3.55 Å is larger than 10% of the largest atom Zr-Zr pairs, which is 3.24 Å as mentioned before.

Differential scanning calorimetry measurements revealed an energy absorption of 0.79 W/g during the glass transition, and an exothermic release of 14.43 W/g during the crystallization. Yet, such of the small energy absorption dramatically changes its mechanical properties, such as that the yield strengths are reduced from ~2,000 MPa with limited plastic deformation at room temperature to ~ 70 MPa with superplasticity during

the glass transition around T_g in Zr-based BMGs. How does the small energy absorption change the atomic structure of BMGs and result in the liquid-like mechanical properties? We try to visualize this change from the consideration of the atomic bonding behavior.

During increasing temperatures, some atom pairs, which have an atomic bonding length shorter than r_1 , have their bonding length increased and enter into the r_1 to r_2 range. Similarly some of them, which have the atomic bonding length in the range of r_1 and r_2 , have their bonding length being larger than r_2 , thus they get out of the r_1 and r_2 range, as illustrated in Fig. 5(b). When there is a net flow of atomic pairs out of the r_1 - r_2 range, free volume is thus increased. From Fig. 5(a) we can see that the $\Delta N/N(RT)$ is largely increased above T_g , with an increase rate of 2.4 ($B_{scl} / B_a = 0.097/0.04$). This suggests that the free volume increases by the rate of 2.4 above the T_g .

Based on the consideration above, the small endothermic energy results in more free volumes, and with the free volume increasing, the tightly-bonded atomic clusters could be separated by the free-volume network, thus turning the entire solid amorphous structure into a liquid-like supercooled liquid structure (See Fig. 6). The regions, where the atomic clusters are interconnected to form a solid skeleton, are dilated into free volume as a result of the small endothermic reaction at T_g , and these regions are defined as interconnecting zones by Fan et al. [21]. According to the tight-bond cluster model, three atomic regions exist in metallic glasses, which are (I) clusters of atoms with strong bonded cores (tightly-bonded atomic clusters); (II) free-volume regions containing loosely bonded atoms; and (III) interconnecting zones with transitional bonding, which bridge the tightly-bonded atomic clusters [21].

Based on the simple tight-bond cluster model, we can further illustrate the glass transition as shown in Fig. 6. The black solid circles represent tight-bonded clusters, and the interconnecting zones are shown as the blue lines. Between these clusters, the longer bond forms free volumes, as indicated by the red dash lines. When the temperature reaches T_g , the bond length of atoms between the clusters becomes significantly dilated as they gain energy, resulting in the formation of additional free volumes. When the clusters are surrounded by a network of free volumes, the glass enters the supercooled liquid state as shown in Fig. 6(b). A comparison of the bond-character change in the interconnecting zone at temperatures below and above T_g is illustrated in Fig. 6(c), which is a superposition of Fig. 6(a) and (b). The changes in the interconnecting zone above T_g not only result in a net free-volume increase [see Fig. 5], but also contribute to increasing the average \bar{r} [see Fig. 4(a)]. From this illustration, we can have an inference that the interconnecting zones with loosely bonded free volumes play a key role in the deformation mechanisms above and below T_g . The interconnecting zone keeps the clusters connected to each other at $T < T_g$, resulting in the formation of BMGs with a high yield strength. At $T > T_g$, interconnecting zones are “dissolved” into the free-volume network, and the solid-like clusters move easily in the liquid-like free-volume matrix, resulting in homogeneous deformation at low applied stresses. Since only transitional bonds break up into free volume, only small energy absorption is involved during the glass transition at T_g .

V. CONCLUSION

In summary, through the *in-situ* x-ray PDF study of the local structure of a metallic glass, we have shown some principal features of the evolution of the local structure of metallic glasses with increasing temperatures from room temperature to above T_g . The changes in the PDF peak shape with temperature are consistent with local density fluctuations, free-volumes are increasing with temperature, and the free volume increasing rate is much higher above T_g . Free volumes form a network matrix above T_g , which separates tight-bonded atomic clusters, is likely the mechanism of the glass transition from the amorphous phase into the supercooled liquid state. It is also likely to provide a physical model to explain the transition from the extremely high yield stress to very low yield stress, and the limited plasticity to supper plasticity during the glass transition around T_g . The atomic level thermal expansion for the nearest atom pairs is most likely to represent the real coefficient due to the anharmonicity of the interatomic potential.

ACKNOWLEDGMENTS

C. Fan thanks J.J Wall for his help in technical discussion. This work was supported by the NSFC (Grant No. 50971057), NSF (DMR-0231320, CMMI-0900271 and DMR-0909037) and benefited from the use of NPDF at Los Alamos National Lab (DOE: W-7405-ENG-36). Use of the Advanced Photon Source was supported by Office of Science, Office of Basic Energy Sciences (OBES), the U.S. DOE (DE-AC02-CH11357). T. Egami was supported by the Division of Mater. Sci. & Eng., Office of Basic Energy Sciences, Department of Energy. C. T. Liu was supported partially by the internal funding from Hong Kong Polytechnic University.

- 1 P. G. Debenedetti and F. H. Stillinger, *Nature* **410**, 259 (2001).
- 2 R. J. Highmore and A. L. Greer, *Nature* **339**, 363 (1989).
- 3 M. D. Ediger, *Journal of Physical Chemistry* **100**, 13200 (1996).
- 4 A. Inoue, *Bulk Amorphous Alloys: Preparation and Functional Characteristics*,
1998).
- 5 W. L. Johnson, *Intermetallic Compounds*, Vol. 1., New York, Wiley, 687 (1994).
- 6 K. S. Lee, T. K. Hab, S. Ahn, et al., *Journal of Non-Crystalline Solids* **317**, 193
(2003).
- 7 O. Mishima and E. S. H., *Nature* **396**, 329 (1998).
- 8 S. Sastry, P. G. Debenedetti, and F. H. Stillinger, *Nature* **393**, 554 (1998).
- 9 A. L. Greer, *Science* **267**, 1947 (1995).
- 10 Y. H. Liu, G. Wang, R. J. Wang, et al., *Science* **315**, 1385 (2007).
- 11 Z. P. Lu, C. T. Liu, J. R. Thompson, et al., *Physical Review Letters* **92**, 245503
(2004).
- 12 G. Sheng, Z. P. Lu, and C. T. Liu, *Intermetallics* **18**, 883 (2010).
- 13 X. Qiu, J. W. Thompson, and S. J. L. Billinge, *J. Appl. Cryst.* **37**, 678 (2004).
- 14 P. F. Peterson, M. Gutmann, T. Proffen, et al., *Journal of Applied Crystallography*
33, 1192 (2000).
- 15 F. Lindemann, *Z. Phys* **11**, 609 (1910).
- 16 M. H. Cohen and G. S. Grest, *Phys. Rev. B* **20**, 1077 (1979).
- 17 T. Egami, S. J. Poon, Z. Zhang, et al., *Phys. Rev. B* **76**, 024203 (2007).
- 18 M. H. Cohen and D. Turnbull, *J. Chem. Phys.* **31**, 1164 (1959).

- ¹⁹ C. Fan, P. K. Liaw, T. W. Wilson, et al., *Appl. Phys. Lett.* **89**, 231920 (2006).
- ²⁰ C. Fan, P. K. Liaw, T. Wilson, et al., *Appl. Phys. Lett.* **89**, 111905 (2006).
- ²¹ C. Fan, P. K. Liaw, and C. T. Liu, *Intermetallics* **17**, 86 (2009).
- ²² C. Fan, P. K. Liaw, V. Haas, et al., *Physical Review B* **74**, 014205 (2006).
- ²³ D. Srolovitz, K. Maeda, S. Takeuchi, et al., *Journal of Physics F-Metal Physics* **11**, 2209 (1981).
- ²⁴ T. Egami, K. Maeda, and V. Vitek, *Phil. Mag.* **41**, 883 (1980).
- ²⁵ T. Egami, D. Maeda, D. Srolovitz, et al., *J. de Phys.* **41**, C8 (1980).

Figure Captions

Figure 1. A schematic diagram for the heating device used to control the sample temperature for synchrotron x-ray diffraction, together with a 2-D image pattern recorded on the image plate detector.

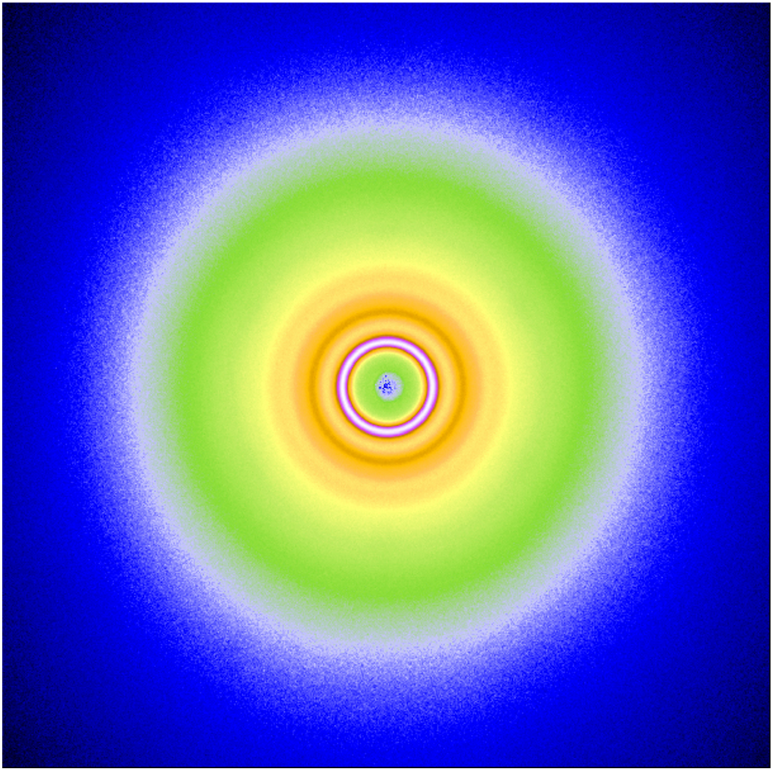
Fig. 2 The structure function, $S(Q)$, of $Zr_{55}Cu_{35}Al_{10}$ BMGs measured *in-situ* by synchrotron x-ray scattering: (a) $S(Q)$ measured at room temperature and 450 °C; (b) $S(Q)$ in the as cast state and after only partial crystallization measured at room temperature.

Fig. 3 The nearest neighbor peaks of the reduced PDFs of $Zr_{55}Cu_{35}Al_{10}$: (a) *in-situ* measured by synchrotron x-ray scattering at *RT* and at 450 °C ($T_g < T < T_x$) for the BMG; (b) measured by neutron scattering at room temperature for the as-cast BMG and its crystallized counterpart (annealed for 1.8 ks at about 700 °C)..

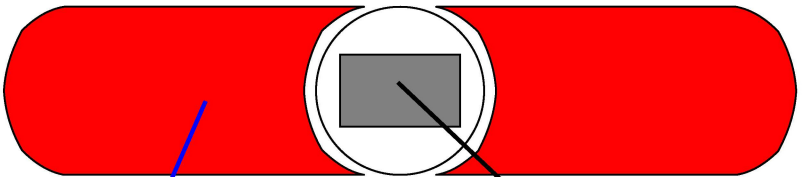
Fig. 4 (a) Relative change in the nearest neighbor distance, $\Delta \bar{r} / \bar{r}_0$, as a function of temperature, here $\Delta \bar{r} = \bar{r} - \bar{r}_0$, \bar{r} : the average nearest pair distance from 2.14 to 3.89 Å in the RDF. $R(r)$ curves were calculated by a center-of-mass method shown as a solid dot, inset (b); \bar{r}_0 : the value at *RT*.

Fig. 5 (a) Changes in the areas of the first peak of the RDF, $\Delta N/N_0$, as a function of temperature, where $\Delta N = N(T) - N_0$, N : the area of the RDF first peak from 3.55 to 3.89 Å, N_0 : the value at room temperature. (b) Illustration of atom pairs move in and out of the r_1 to r_2 range when the temperature changes.

Fig. 6 (a), (b), and (c) a schematic showing the structural change at the glass transition: a change in the connections between clusters below and above T_g (black: below T_g and red: above T_g).



To image plate



Heating device

Sample

Incident photons

